CRYSTAL GROWTH & DESIGN

Article

pubs.acs.org/crystal

High-Quality Epitaxy of Ruthenium Dioxide, RuO_2, on Rutile Titanium Dioxide, TiO_2, by Pulsed Chemical Vapor Deposition

Xinwei Wang[†,‡] and Roy G. Gordon[†,*]

[†]Department of Chemistry and Chemical Biology, Harvard University, Cambridge, Massachusetts 02138, United States

[‡]School of Advanced Materials, Peking University Shenzhen Graduate School, Shenzhen 518055, China

ABSTRACT: Pulsed chemical vapor deposition was used to prepare epitaxial ruthenium dioxide (RuO_2) film on rutile TiO_2 (011) at low temperature 280 °C. Reciprocal space mapping by high-resolution X-ray diffraction was used to examine the quality of epitaxy, which demonstrated a high quality epitaxy of the deposited RuO_2 film. The results also showed that the RuO_2 lattice was fully strained by the substrate in the lateral directions and, therefore, distorted from a tetragonal to a monoclinic structure.

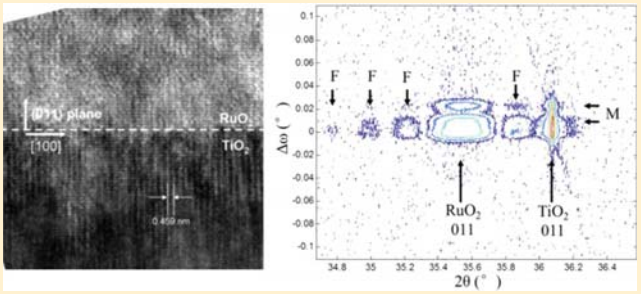

INTRODUCTION

RuO_2 is a transition metal oxide that has many unique properties. It has metallic conductivity at room temperature and a high work function, which makes it suitable as an electrode material for field emission cathodes[1] and dynamic random access memory (DRAM).[2] RuO_2 has the rutile structure with lattice constants that are very similar to those of rutile TiO_2, a material with a high dielectric constant. Therefore, capacitors with high capacitance per unit area have been achieved by a stack structure of $RuO_2/TiO_2/RuO_2$.[3] In forming this structure, RuO_2 substrates induce TiO_2 to grow epitaxially in its rutile form with a high dielectric constant, rather than in its anatase form with a lower dielectric constant. The high work function of RuO_2 makes these capacitors have low leakage current. Due to its good redox properties, RuO_2 has been made into electrodes for supercapacitors.[4−6] Also, RuO_2 has a relatively small magneto-resistance, and therefore it has been used in cryogenic temperature sensors.[7,8] Moreover, RuO_2 has been extensively studied as a catalyst for oxidation of CO,[9−11] HCl,[12] and an electrocatalyst for chlorine evolution[13,14] and oxygen evolution[15] during electrolysis. In industry, RuO_2 is the main active component in TiO_2-based dimensionally stable anodes (DSA), widely used in chlorine production.[16] Ultrathin RuO_2 supported on TiO_2 rutile forms an efficient and stable catalyst for gas-phase oxidation of HCl, which has been implemented for large-scale production of chlorine.[17] Several studies have followed to investigate the mechanism of this RuO_2/TiO_2 catalyst.[18,19]

The RuO_2/TiO_2 interface is important in many of these applications, but its detailed structure and properties are unknown. The RuO_2/TiO_2 interface has been reported to be unstable above 400 °C, when RuO_2 and TiO_2 begin to interdiffuse to form a $Ti_{(1-x)}Ru_xO_2$ alloy at their (110) interface.[20,21] Moreover, the (011) surface of TiO_2 is even less thermodynamically stable than the (110) surface, as the (011) surface reconstructs at 800 °C.[22] This suggests that a low-temperature growth process would be necessary for epitaxial growth of RuO_2 on TiO_2. Chemical vapor deposition (CVD) can make epitaxial films that are thermally or in vacuo unstable, such as ferromagnetic CrO_2.[23] If the chemical precursors are chosen properly, the CVD reaction temperature can be low, for example in the range of 100−300 °C.[24] A number of other oxide films have been made by CVD, such as wide-gap semiconductors ZnO[23,25] and SnO_2,[26,27] superconducting oxides,[28] and oxide gate electrode materials.[29] Also, a costly ultrahigh vacuum chamber is not necessary for CVD, which is usually run in a low vacuum level or at atmospheric pressure, where it is scalable to very large areas, such as coating window glass.[24]

To provide information about the RuO_2/TiO_2 interface, we grew single crystal films of RuO_2 epitaxially on single-crystal TiO_2 substrates using a new CVD process. The RuO_2 was grown at a substrate temperature of 280 °C by pulsed-CVD at low pressure. At this low temperature, no measurable interdiffusion occurs, so the RuO_2/TiO_2 interface remains abrupt. We chose to grow RuO_2 on rutile TiO_2 (011) surfaces, since the (011) plane has relatively small lattice mismatches of −2.0% along the [100] direction, and +0.07% along the $[01\bar{1}]$ direction.

The resulting RuO_2/TiO_2 (011) structures were characterized in great detail by reciprocal space mapping using high-resolution X-ray diffraction (HRXRD), facilitated by the similar lattice structures of RuO_2 and TiO_2. Reciprocal space mapping is a very useful method to examine the structure and the quality of epitaxy. By using the reciprocal lattice of the substrate as the internal reference, and locating the relative peak positions from

Received: December 7, 2012
Revised: January 24, 2013
Published: February 1, 2013

the film, we were able to construct the reciprocal lattice of the film to very high accuracy and to understand its small lattice distortions by the TiO_2 substrate and its lattice alignment relative to the substrate. Usually, this type of analysis has been performed on a cubic structure film grown on (100) of a cubic structure substrate (e.g., Si, Ge, and GaAs), in which there is a 4-fold symmetry about the axis perpendicular to the surface. This 4-fold symmetry restricts the possibilities of the lattice distortion of the film: only two degrees of freedom are allowed (i.e., one for lateral and one for perpendicular), so that it is only possible for the cubic structure film to distort into a tetragonal structure, which retains the 4-fold symmetry at its square base. Therefore, in theory, taking reciprocal space maps of the symmetric peak and any one of the asymmetric peaks is enough for the information to solve the entire reciprocal lattice profile. However, our RuO_2 film was grown on the (011) surface of the tetragonal TiO_2 substrate. This (011) plane does not have 4-fold symmetry, which severely complicates the analysis process. The distortion of RuO_2 can occur differently in two orthogonal lateral directions. Therefore, mapping information of the reciprocal lattice points in both orthogonal lateral directions is necessary. Through a careful HRXRD analysis described below, we successfully solved the distorted structure of the RuO_2 film, and we found that it was a high-quality epitaxial RuO_2 film grown on the TiO_2 (011) substrate. The thin RuO_2 film is constrained to match the lattice constants of the TiO_2 substrate in the two planar directions, while the RuO_2 is partially relaxed in the direction perpendicular to the substrate, resulting in a slight monoclinic distortion of the film.

EXPERIMENTAL SECTION

The RuO_2 films were grown by pulsed CVD in a home-built tube reactor, with bis(*N,N′*-di-*tert*-butylacetamidinato)ruthenium(II) dicarbonyl[30−32] as the ruthenium precursor and oxygen as the coreactant gas. The ruthenium precursor was placed in a glass bubbler in an oven at 140 °C, and it was delivered into the reactor tube with nitrogen carrier gas during each precursor pulse. A gas mixture of oxygen and nitrogen (O_2:N_2 = 1:2 in partial pressure) was kept flowing at a total pressure of 0.45 Torr, while the ruthenium precursor was delivered. Five hundred pulses of the ruthenium precursor were supplied to grow a RuO_2 film. Rutile TiO_2 (011) substrates supplied by MTI Corporation were used for growing epitaxial RuO_2 films. We also used thermal SiO_2 substrates for comparison. Each substrate was treated with UV/ozone for 5 min to remove surface organic contaminants before deposition. The deposition temperature was 280 °C.

The crystal structure of epitaxial RuO_2 film was examined by high-resolution X-ray diffraction (HRXRD) (Bruker D8 HRXRD). The incident beam for HRXRD (Cu Kα_1) was monochromated by a Ge (022) × 4 asymmetric monochromator and a scintillation point detector (Pathfinder) with a Ge (022) × 3 analyzer inserted was used to collect the X-ray signal. The RuO_2/TiO_2 interface was examined by cross-sectional transmission electron microscopy (TEM) (JEOL 2100). The film surface roughness was examined by atomic force microscopy (AFM) (Asylum, Model MFP-3D).

RESULTS AND DISCUSSION

We first used HRXRD to examine the crystal structure of the RuO_2-on-TiO_2 sample. The sample was first aligned in the (φ = 0°) configuration, where TiO_2 [100] was coplanar with the incident and exit X-ray beams, as shown in Figure 1 a. We chose to perform the out-of-plane reciprocal space mappings (scanning ω and 2θ) of the 011 and 222 reflections. (The 111 reflection is not allowed in the Bragg reflection geometry with this configuration.) Then, we rotated the sample by ±90°, so

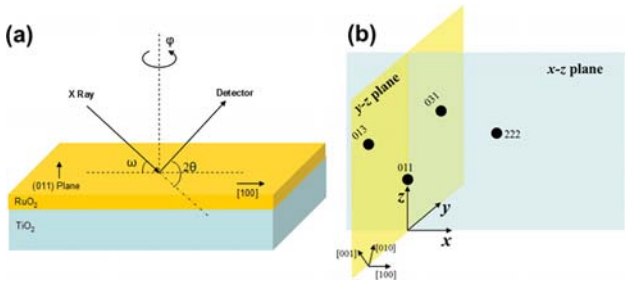

Figure 1. (a) Experimental configuration of HRXRD. (b) Schematic illustration of reciprocal space mappings.

that we could perform the out-of-plane reciprocal space mappings in the orthogonal plane (not shown in Figure 1a. In this configuration (φ = ± 90°), we chose the 011, 031, and 013 reflections, since many other low miller index planes are not allowed in the Bragg reflection geometry.

Notice that, unlike cubic structure, for a tetragonal structure, [011] is not the normal direction of the (011) plane, therefore, in order to avoid confusion, we will discuss our results mainly in the reciprocal space, since the reciprocal space mapping technique gives direct information in reciprocal space. We further define the coordinates in reciprocal space in the substrate reference frame as follows: x is the direction of [100], z is the normal direction of the (011) plane, and y is the direction of $z \times x$ (Figure 1b). Therefore, the previously mentioned measurements correspond to the (q_x,q_z) area mappings of the 011 and 222 reflections in the xz plane (ϕ = 0° configuration) and the (q_y,q_z) area mappings of the 011, 031, and 013 reflections in yz plane (ϕ = ± 90° configuration), respectively. With the fine reciprocal space structure of two orthogonal planes, we expected to construct the whole three-dimensional reciprocal lattice profile.

The reciprocal space maps of the symmetric 011 reflection are shown in Figure 2 (a, b). Two maps correspond to two perpendicular projections of the three-dimensional lattice profile in reciprocal space on the xz and yz planes, respectively. The intensity contours are shown on a logarithmic scale. Along with the TiO_2 011 peak, both the RuO_2 011 main peak and its thickness fringes (denoted as "F" in Figure 2) were clearly observed, which suggested that it was a high-quality epitaxial growth of RuO_2 on TiO_2 (011). With the use of the TiO_2 011 peak as the internal reference, the 2θ value of the RuO_2 011 main peak was 35.5421°. Comparing it with the reference value of 35.0505° (PDF 00-040-1290) measured from a bulk crystal, we found that the peak position shifted by ∼0.49° due to the distortion imposed by the TiO_2 substrate. There were also a few detailed features we noticed in these two reciprocal space maps. First, the TiO_2 substrate was not a perfect single crystal; it had several mosaic blocks as shown as satellite peaks in the $\Delta\omega$-axis direction (denoted as "M" in Figure 2), which corresponds to sample rocking ($\Delta\omega$ is the sample tilting angle). And, interestingly, the RuO_2 peaks also showed correlated satellite peak shapes in the $\Delta\omega$-axis direction, which suggested that our RuO_2 film was epitaxially grown on each individual block of TiO_2. Besides, the spreading of the RuO_2 011 main peak in the $\Delta\omega$-axis direction was very close to that of the substrate peak, which again suggested a high quality of epitaxy. We further noticed that, in Figure 2a, the RuO_2 peaks were not exactly located on the $\Delta\omega$ = 0 line. This was due to a small miscut of our TiO_2 substrate. Since the direction defined by the film main peak and thickness fringes is the

dx.doi.org/10.1021/cg301801h | *Cryst. Growth Des.* 2013, 13, 1316−1321

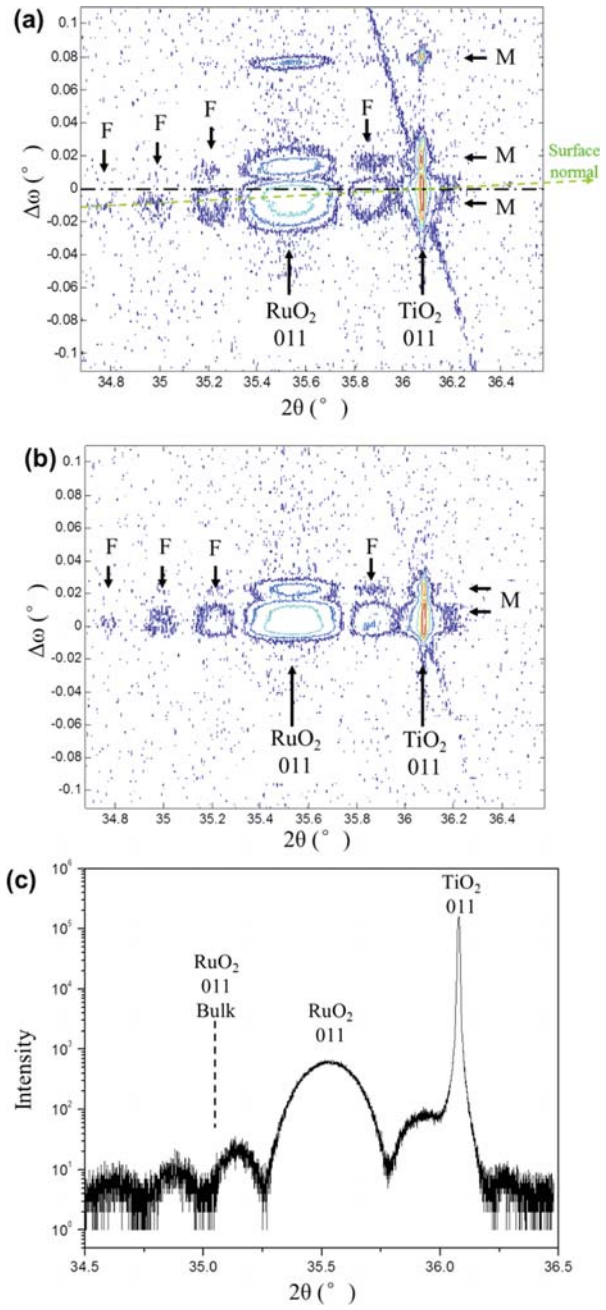

Figure 2. Reciprocal space maps of the 011 reflection in the (a) *xz* plane and (b) *yz* plane. "F" and "M" denote the satellite peaks due to thickness fringes and mosaic blocks, respectively. (c) Coupled $\omega-2\theta$ scan of the 011 reflection. The 011 peak position for bulk RuO_2 is also shown for comparison.

physical surface normal direction, and the $\Delta\omega = 0$ line corresponds to the normal direction of the crystal lattice plane, the angle between these two directions corresponds to the miscut angle of the substrate, which was calculated to be ~0.3°. Furthermore, the TiO_2 011 peak was collinear with RuO_2 011 main peak and its fringes, which provided the information regarding the growth direction of the RuO_2 film. We will come back to discuss this later in this paper. Nevertheless, we will neglect this small miscut angle for now, and the error of neglecting will be discussed later. In addition, the thickness of the RuO_2 film can be extracted from the periodicity of the thickness fringes. In order to have a better fitting, we performed a coupled $\omega-2\theta$ scan with smaller step size and longer collecting time with a $\phi = 90°$ configuration. The data are plotted in Figure 2c, and the film thickness was determined to be ~38 nm.

Then, we performed the reciprocal space mappings of the asymmetric 222, 031, and 013 reflections to obtain the reciprocal lattice profile in both the *xz* and the *yz* planes, which would lead us to understand the full lattice structure of the RuO_2 film grown on TiO_2 (011). The (q_x,q_z) area mapping of the 222 reflection is shown in Figure 3, and the (q_y,q_z) area

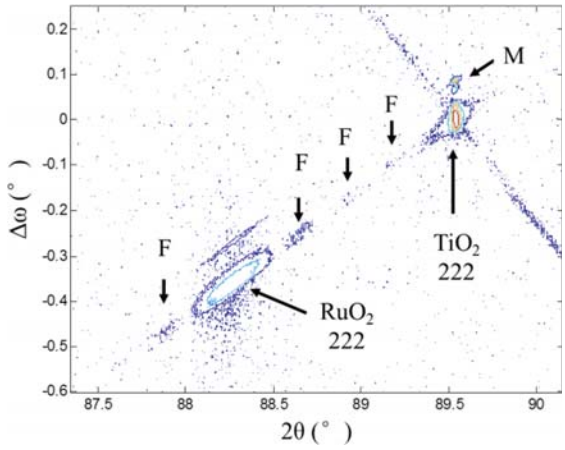

Figure 3. Reciprocal space map of the 222 reflection in *xz* plane. "F" and "M" denote the satellite peaks due to thickness fringes and mosaic blocks, respectively.

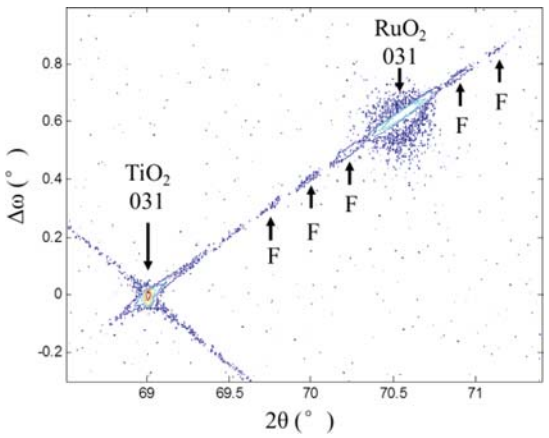

Figure 4. Reciprocal space map of the 031 reflection in the *yz* plane. "F" denotes the satellite peaks due to thickness fringes.

mappings of the 031 and 013 reflections are shown in Figures 4 and 5, respectively. The peak position of the RuO_2 222 reflection was observed at $\Delta\omega = -0.3562°$ and $2\theta = 88.2871°$ in Figure 3, the peak position of RuO_2 031 reflection was observed at $\Delta\omega = 0.6271°$ and $2\theta = 70.5549°$ in Figure 4, and the peak position of RuO_2 013 reflection was observed at $\Delta\omega = -0.8080°$ and $2\theta = 100.7082°$ in Figure 5. In these three figures, similar fine features of the contour shape are observed as in Figure 1: satellite peaks in the $\Delta\omega$-axis direction, which correspond to the mosaic blocks of the substrate TiO_2, similar widths of the peak spreadings in the $\Delta\omega$-axis direction for both

dx.doi.org/10.1021/cg301801h | *Cryst. Growth Des.* 2013, 13, 1316−1321

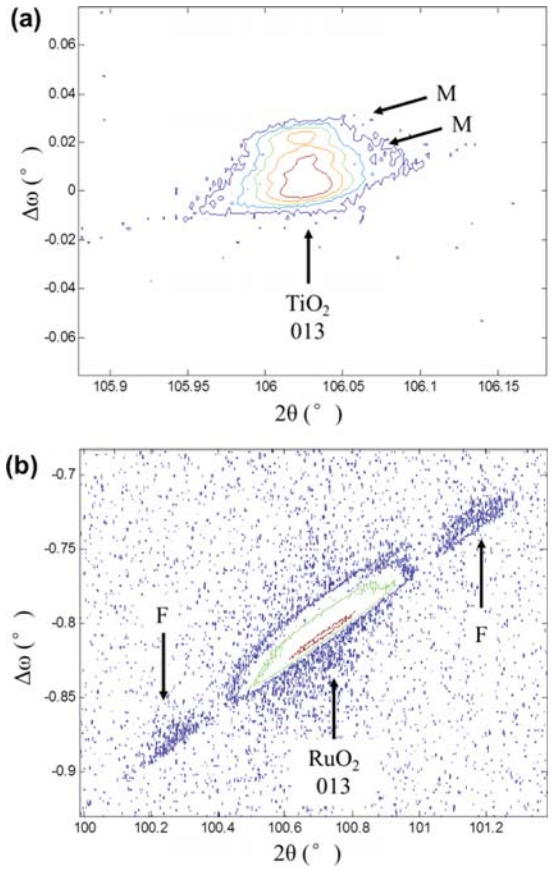

Figure 5. Reciprocal space maps of the 013 reflections of (a) the TiO_2 substrate and (b) the RuO_2 film in the *yz* plane. "F" and "M" denote the satellite peaks due to thickness fringes and mosaic blocks, respectively. Notice that (a) and (b) are on different scales.

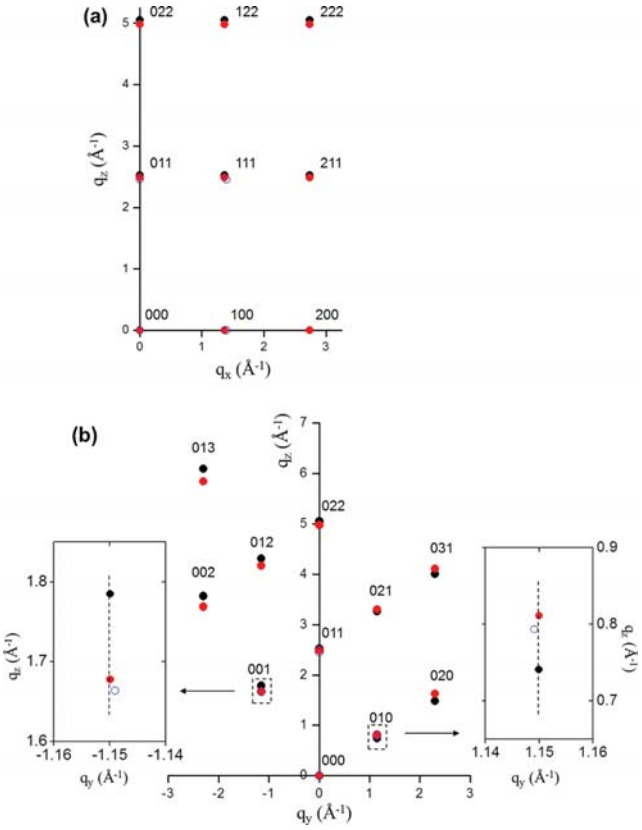

Figure 6. Reciprocal lattice profile of the RuO_2 film (red dots) and the TiO_2 substrate (black dots) in the (a) the *xz* plane and (b) *yz* plane. For comparison, the unstrained (bulk) RuO_2 reciprocal lattice was also plotted (open blue circles).

the substrate and the film main peaks, and clear thickness fringes and the collinearity of the film main peak, thickness fringes, and the substrate main peak. All of these observations again indicated a high-quality epitaxy of RuO_2 grown on TiO_2 (011).

In combination with the peak positions of the RuO_2 011, 222, 031, and 013 reflections, we were able to construct the reciprocal lattice structure of the RuO_2 film with respect to that of the TiO_2 substrate. Reciprocal lattice patterns in the *xz* and *yz* planes are shown in Figure 6 (panels a and b, respectively). As the patterns indicated, the RuO_2 lattice was fully pinned by the substrate laterally: each of the film reciprocal lattice points was right below its corresponding substrate reciprocal lattice point. Only the direction normal to the surface had some degree of relaxation. Moreover, we found the angle between the (010) and (001) reflections was 89.23°, which is slightly distorted from a right angle. Thus, the RuO_2 film lost its tetragonal symmetry and became a monoclinic structure, although the difference is not large. In addition, since the film's main peak and its thickness fringes determine the normal direction of the surface, this fully pinned structure was also consistent with the collinearity we observed in Figures 2−5. Finally, the RuO_2 film grown on TiO_2 (011) had a monoclinic structure, with lattice parameters of a = 4.5933 Å, b = 4.4647 Å, c = 3.0889 Å, and α = 89.23°. Notice that the lattice constant a of RuO_2 was stretched to be equal to that of TiO_2, due the lateral pinning effect imposed by the substrate.

In the following, we would like to discuss the effect of the small miscut as mentioned previously. First of all, we will only discuss the effect of the miscut in the [100] direction, which corresponded to the reciprocal space mapping of the *xz* plane (Figure 2a), since in the *yz* plane, the miscut effect was almost unobservable as shown in Figure 2b. Noticing that the film was fully pinned by the substrate, the effect of the small miscut we observed led to a small rotation of the RuO_2 reciprocal space profile with respect to the substrate profile. As a result, the RuO_2 011 reciprocal lattice point shifted laterally as shown in Figure 7. For this sample, the shift was 0.0002 $Å^{-1}$ based on our reciprocal space mapping data of the 011 reflection. And this corresponded to a 0.0046° of rotation of the RuO_2 lattice in the reciprocal space. Then, we used this rotation value to predict the lateral shift of the RuO_2 222, which was calculated to be

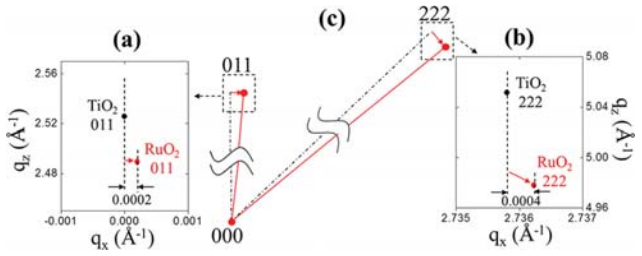

Figure 7. Blow up of the reciprocal lattice profile near (a) 011 and (b) 222 in the *xz* plane. (c) Schematic illustration of the effect of the miscut.

dx.doi.org/10.1021/cg301801h | Cryst. Growth Des. 2013, 13, 1316−1321

0.0004 $Å^{-1}$. This value was exactly the same as that which we extracted from our experimental data of the reciprocal space map of the 222 reflection. Indeed, the effect of the miscut was observable by our measurements; the effect of this small miscut was very small, and its influence on the peak positions of the RuO_2 031 and 013 reflections was also negligible. Nevertheless, this miscut caused the rotation in reciprocal space. However, we propose that if the RuO_2 film is grown on a zero-miscut TiO_2 (011) substrate, there will be no rotation in reciprocal space; each pair of the reciprocal lattice points of the RuO_2 and TiO_2 will be perfectly aligned in the normal direction of the surface.

The above HRXRD results indicated that the RuO_2 grown on TiO_2 was a high-quality epitaxy with a lateral fully pinned structure. In particular, the clear thickness fringes suggested a smooth surface and a low level of defects of the RuO_2 film. We further examined the surface by AFM and the interface of RuO_2 and TiO_2 by cross-sectional TEM. The AFM (Figure 8) results

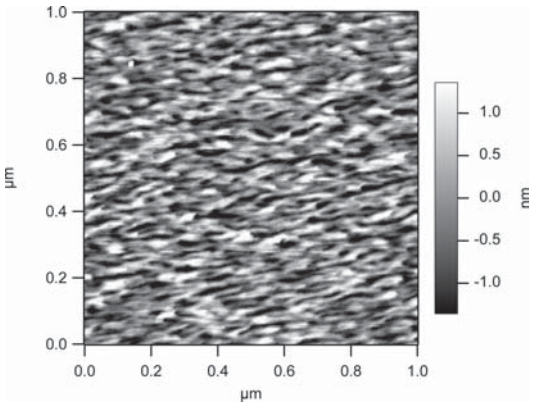

Figure 8. AFM image of the RuO_2 film surface.

confirmed the smoothness of the film, with an rms roughness value of only 0.78 nm for a 40 nm film. And the TEM image (Figure 9) showed a perfect alignment of the RuO_2 and TiO_2 lattices. Also, no interfacial layer was observed. These good properties can be attributed to the low temperature pulsed CVD process. At the process temperature of 280 °C, the interdiffusion rates of Ru and Ti atoms are very slow, while the

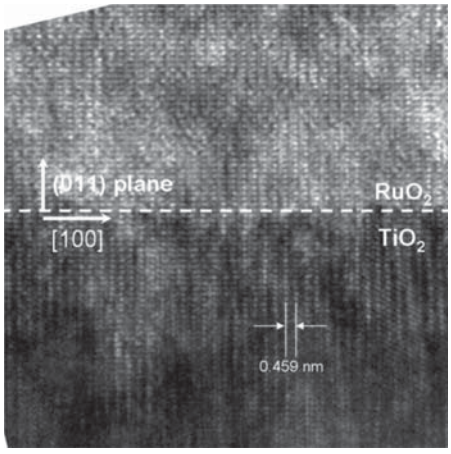

Figure 9. Cross-sectional TEM of the RuO_2/TiO_2 interface.

surface mobility of Ru atoms is still high, probably with help from the ligand and/or coreactant oxygen.

CONCLUSIONS

In this work, we presented a low-temperature pulsed CVD process to grow epitaxial RuO_2 thin films on TiO_2 (011) substrates. The epitaxy structure was examined by HRXRD. We collected the reciprocal space maps of the 011, 222, 031, and 013 reflections. The clear thickness fringes and small spreading of the film peaks both show the high quality of the epitaxy. Using the diffraction peak positions of RuO_2 and TiO_2, we were able to construct the reciprocal lattice of RuO_2. The result demonstrated that the RuO_2 film was fully pinned by the TiO_2 substrate in both lateral directions, forming a single-crystalline, monoclinic epitaxial film.

AUTHOR INFORMATION

Corresponding Author

*E-mail: gordon@chemistry.harvard.edu.

Notes

The authors declare no competing financial interest.

ACKNOWLEDGMENTS

X.W. would like to thank Dr. Scott A. Speakman at MIT for discussion of HRXRD data analysis. Dow Chemical Company supplied the ruthenium amidinate precursor. This work was performed in part at Harvard University's Center for Nanoscale Systems (CNS), a member of the National Nanotechnology Infrastructure Network (NNIN).

REFERENCES

(1) Hsieh, C. S.; Wang, G.; Tsai, D. S.; Chen, R. S.; Huang, Y. S. *Nanotechnology* **2005**, *16*, 1885.
(2) Park, S. E.; Kim, H. M.; Kim, K. B.; Min, S. H. *J. Electrochem. Soc.* **2000**, *147*, 203.
(3) Frohlich, K.; Tapajna, M.; Rosova, A.; Dobrocka, E.; Husekova, K.; Aarik, J.; Aidla, A. *Electrochem. Solid-State Lett.* **2008**, *11*, G19.
(4) Zhang, J. T.; Ma, J. Z.; Zhang, L. L.; Guo, P. Z.; Jiang, J. W.; Zhao, X. S. *J. Phys. Chem. C* **2010**, *114*, 13608.
(5) Hu, C. C.; Chang, K. H.; Lin, M. C.; Wu, Y. T. *Nano Lett.* **2006**, *6*, 2690.
(6) Zheng, J. P.; Cygan, P. J.; Jow, T. R. *J. Electrochem. Soc.* **1995**, *142*, 2699.
(7) Sahul, R.; Tasovski, V.; Sudarshan, T. S. *Sens. Actuators, A* **2006**, *125*, 358.
(8) Watanabe, M.; Morishita, M.; Ootuka, Y. *Cryogenics* **2001**, *41*, 143.
(9) Over, H.; Kim, Y. D.; Seitsonen, A. P.; Wendt, S.; Lundgren, E.; Schmid, M.; Varga, P.; Morgante, A.; Ertl, G. *Science* **2000**, *287*, 1474.
(10) Knapp, M.; Seitsonen, A. P.; Kim, Y. D.; Over, H. *J. Phys. Chem. B* **2004**, *108*, 14392.
(11) Wang, H. Y.; Schneider, W. F. *Phys. Chem. Chem. Phys.* **2010**, *12*, 6367.
(12) Crihan, D.; Knapp, M.; Zweidingey, S.; Lundgren, E.; Weststrate, C. J.; Andersen, J. N.; Seitsonen, A. P.; Over, H. *Angew. Chem., Int. Ed.* **2008**, *47*, 2131.
(13) Hansen, H. A.; Man, I. C.; Studt, F.; Abild-Pedersen, F.; Bligaard, T.; Rossmeisl, J. *Phys. Chem. Chem. Phys.* **2010**, *12*, 283.
(14) Ryan, J. V.; Berry, A. D.; Anderson, M. L.; Long, J. W.; Stroud, R. M.; Cepak, V. M.; Browning, V. M.; Rolison, D. R.; Merzbacher, C. I. *Nature* **2000**, *406*, 169.
(15) Petrykin, V.; Macounova, K.; Shlyakhtin, O. A.; Krtil, P. *Angew. Chem., Int. Ed.* **2010**, *49*, 4813.
(16) Trasatti, S. *Electrochim. Acta* **2000**, *45*, 2377.

(17) Iwanaga, K.; Seki, K.; Hibi, T.; Issoh, K.; Suzuta, T.; Nakada, M.; Mori, Y.; Abe, T. *Sumitomo Kagaku (Osaka, Jpn.)* **2004**, *I*, 1.
(18) Seitsonen, A. P.; Over, H. *J. Phys. Chem. C* **2010**, *114*, 22624.
(19) Hevia, M. A. G.; Amrute, A. P.; Schmidt, T.; Perez-Ramirez, J. *J. Catal.* **2010**, *276*, 141.
(20) Rizzi, G. A.; Magrin, A.; Granozzi, G. *Phys. Chem. Chem. Phys.* **1999**, *1*, 709.
(21) Kim, Y. J.; Gao, Y.; Chambers, S. A. *Appl. Surf. Sci.* **1997**, *120*, 250.
(22) Kubo, T.; Orita, H.; Nozoye, H. *J. Am. Chem. Soc.* **2007**, *129*, 10474.
(23) Chambers, S. A. *Adv. Mater.* **2010**, *22*, 219.
(24) Gordon, R. *J. Non-Cryst. Solids* **1997**, *218*, 81.
(25) Liang, H.; Gordon, R. G. *J. Mater. Sci.* **2007**, *42*, 6388.
(26) Heo, J.; Hock, A. S.; Gordon, R. G. *Chem. Mater.* **2010**, *22*, 4964.
(27) Gordon, R. G.; Proscia, J.; Ellis, F. B., Jr.; Delahoy, A. E. *Sol. Energy Mater.* **1989**, *18*, 263.
(28) Watson, I. M. *Chem. Vap. Deposition* **1997**, *3*, 9.
(29) Frohlich, K.; Husekova, K.; Machajdik, D.; Hooker, J. C.; Perez, N.; Fanciulli, M.; Ferrari, S.; Wiemer, C.; Dimoulas, A.; Vellianitis, G.; Roozeboom, F. *Mater. Sci. Eng., B* **2004**, *109*, 117.
(30) Li, H.; Farmer, D. B.; Gordon, R. G.; Lin, Y.; Vlassak, J. *J. Electrochem. Soc.* **2007**, *154*, D642.
(31) Li, H.; Aaltonen, T.; Li, Z.; Lim, B. S.; Gordon, R. G. *Open Inorg. Chem. J.* **2008**, *2*, 11.
(32) Wang, H.; Gordon, R. G.; Alvis, R.; Ulfig, R. M. *Chem. Vap. Deposition* **2009**, *15*, 312.